Influence of type of wave and angle of incidence on seismic bending moments in pile foundations *

J.M. Zarzalejos, J.J. Aznárez, L.A. Padrón and O.Maeso
Instituto Universitario de Sistemas Inteligentes y Aplicaciones Numéricas en Ingeniería (SIANI) Universidad de Las Palmas de Gran Canaria
Edificio Central del Parque Científico y Tecnológico
Campus Universitario de Tafira, 35017, Las Palmas de Gran Canaria, Spain
{jmzarzalejos,jjaznarez,lpadron,omaeso}@siani.es

2014

Abstract

When analysing the seismic response of pile groups, a vertically–incident wavefield is usually employed even though it does not necessarily correspond to the worst case scenario. This work aims to study the influence of both the type of seismic body wave and its angle of incidence on the dynamic response of pile foundations. To this end, the formulation of SV, SH and P obliquely–incident waves is presented and implemented in a frequency–domain boundary element–finite element code for the dynamic analysis of pile foundations and piled structures. Results are presented in terms of bending moments at cap level of single piles and 3×3 pile groups, both in frequency and in time domain. It is found that, in general, the vertical incidence is not the most unfavorable situation. In particular, obliquely–incident SV waves with angles of incidence smaller than the critical one, situation in which the mechanism of propagation of the waves in the soil changes and surface waves appear, yield bending moments much larger than those obtained for vertically–incident wavefields. It is also shown that the influence of pile–to–pile interaction on the kinematic bending moments becomes significant for non–vertical incidence, especially for P and SV waves.

1 Introduction

The dynamic response of single piles and pile groups is a topic of great interest that has been extensively studied during the last forty years. However, some aspects of the problem are not yet well understood and hence require more investigation. Among others, the characterisation of the excitation is usually simplified considering only a vertically–incident wavefield. When a stratified medium is considered, and provided that the stiffness of the different layers increases with depth, the refraction processes which take place as the incident waves travel through the layers tend to make them impinge on the ground surface almost vertically. Nevertheless, the seismic actions are, in general, composed of a combination of waves which propagate with an angle of incidence not necessarily vertical [1].

The main aim of this paper is to investigate the influence of the type of incident wave and of its angle of incidence on the dynamic response of pile foundations embedded in a homogeneous halfspace. To this end, bending moments at pile heads will be estimated and compared both in frequency and in time domain.

The response of single piles of different properties to obliquely incident body waves was studied for the first time in the pioneer work by Mamoon and Ahmad [2] by means of the kinematic interaction factors of the foundations. This paper was the starting point for the following work by Mamoon and Banerjee [3], where the response of single piles and pile groups to travelling SH waves was investigated. Makris and Badoni [4] also studied this problem for Rayleigh and obliquely–incident SH waves making use of a Winkler–type approach. However, the most comprehensive study can be found in the work by Kaynia and Novak [5], where kinematic

*Draft of the paper originally published in Earthquake Engineering and Structural Dynamics 2014; 43:41–59.

interaction factors of different configurations of pile foundations were obtained both for obliquely incident body waves and for Rayleigh waves. In addition, Gazetas *et al.* [6] presented one of the first approaches to the determination of bending moments at pile heads.

This work makes use of a 3–D frequency–domain boundary element–finite element formulation to quantify the influence of type of wave and angle of incidence on bending moments at pile heads. To this end, frequency response functions for the bending moments developed at pile heads of single piles and pile groups are presented for different types of waves and angles of incidence. Special attention is given to the SV case in order to investigate the influence of the arising surface waves. Inertial interaction is also taken into account by the existence of a superstructure. Envelopes of maximum bending moments are also shown for a type 1 elastic response spectrum for ground type C as defined in Part 1 of Eurocode 8 [7]. It is shown that the consideration of non–vertical wavefields and, especially, of obliquely–incident SV waves, yields much larger bending moments than those corresponding to the usually considered vertically–incident S waves.

2 Formulation of incident fields propagating with generic angles of incidence

The objective of this section is to present the governing equations for a planar wavefront propagating through an elastic halfspace with a generic angle of incidence. They will be presented in a format suitable to be used inside a classic boundary element code as the incident field.

When a wave reaches the free surface of the halfspace, other reflected waves must appear in order for the free–field boundary conditions to hold. The displacements in the i^{th} direction (x_i, $i = 1, 2, 3$) of any point of the halfspace can be expressed as the superposition of the effects of the incident and reflected waves. Since the problem is harmonic, and dropping the repeated $e^{i\omega t}$ terms, the displacements can be written as

$$u_i = \sum_{j=1}^{n} b_i^j \, A_j \, e^{-i \, k_j \, (\mathbf{s}^{(j)} \cdot \mathbf{r})} \tag{1}$$

being u_i the component in the i^{th} direction of the total displacement, n the total number of waves of the problem (i.e., the incident plus the reflected waves), b_i^j the component in the i^{th} direction of the vector containing the direction cosines of the displacements produced by the j^{th} wave, A_j the amplitude of the j^{th} wave, k_j the wave number of the j^{th} wave, and $\mathbf{s}^{(j)} \cdot \mathbf{r}$ the dot product of the unit vector defining the direction of propagation of the j^{th} wave (i.e., vector $\mathbf{s}$) and the vector containing the coordinates of the point where the displacements are calculated. Note that while $\mathbf{s}$ denotes the direction of propagation of the wavefront, $\mathbf{b}$ expresses the direction of the particle displacements, and that P and SV waves are associated to in-plane motion in the $x_2 - x_3$ plane while SH waves produce horizontal displacements in the x_1 direction. Also, the direction of the incident wave is defined by the angle θ_o, measured in the $x_2 - x_3$ plane with respect to the horizontal axis x_2 (note that, in most seismological papers, θ_o is defined with respect to the vertical axis x_3). As it is known, when an SH wave reaches the free surface, the reflected wave is a single SH wave. Conversely, if the incident wave is a P or an SV one, then after the process of reflection there appears both a P and an SV wave (see figure 1).

The amplitudes of the reflected waves, shown in table 1, are obtained by assuming unit amplitude incident waves, and applying equilibrium and compatibility conditions at the traction–free surface [8, 9]. The angles of these reflected waves are obtained taking into account that the boundary conditions are independent of the x_2 direction, being θ_1 (angle of the reflected wave of the same type of the incident one) equal to θ_o in all cases, $\theta_2 = cos^{-1}[\kappa^{-1} \cos(\theta_o)]$ for a reflected P wave due to an incident SV wave, and $\theta_2 = cos[\kappa \cos(\theta_o)]$ for a reflected SV wave due to an incident P wave, with $\kappa = c_s/c_p < 1$, $c_s = \sqrt{\mu/\rho}$ and $c_p = \sqrt{\lambda + 2\mu/\rho}$ the velocities of S and P waves, μ and λ the Lamé constants, and ρ the density of the medium.

In the case of an incident SV wave, the angle of incidence causing the cosine of the reflected P wave to have a unit value is called critical angle, having the expression given by eq. (2),

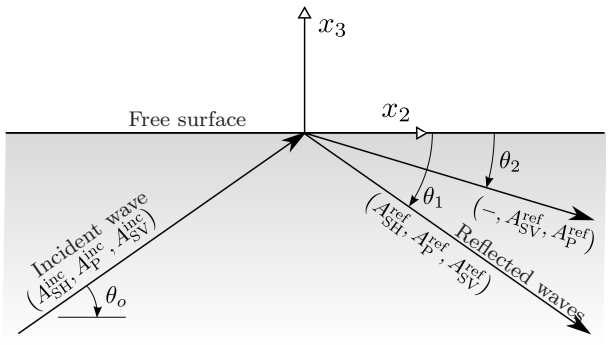

Figure 1: Incident and reflected plane waves in elastic half-space. Definition of angles of the incident and reflected field.

Table 1: Amplitudes of the incident and reflected waves of the problem.

Inc. wave	Waves	A
SH	$\mathrm{SH}^{\mathrm{inc}}$	1
	$\mathrm{SH}^{\mathrm{ref}}$	1
SV	$\mathrm{SV}^{\mathrm{inc}}$	1
	$\mathrm{SV}^{\mathrm{ref}}$	$\dfrac{\kappa^2 \sin(2\theta_o)\sin(2\theta_2) - \cos^2(2\theta_o)}{\kappa^2 \sin(2\theta_o)\sin(2\theta_2) + \cos^2(2\theta_o)}$
	$\mathrm{P}^{\mathrm{ref}}$	$-\dfrac{\kappa \sin(4\theta_o)}{\kappa^2 \sin(2\theta_o)\sin(2\theta_2) + \cos^2(2\theta_o)}$
P	$\mathrm{P}^{\mathrm{inc}}$	1
	$\mathrm{P}^{\mathrm{ref}}$	$\dfrac{\kappa^2 \sin(2\theta_o)\sin(2\theta_2) - \cos^2(2\theta_2)}{\kappa^2 \sin(2\theta_o)\sin(2\theta_2) + \cos^2(2\theta_2)}$
	$\mathrm{SV}^{\mathrm{ref}}$	$\dfrac{2\kappa \sin(2\theta_o)\cos(2\theta_2)}{\kappa^2 \sin(2\theta_o)\sin(2\theta_2) + \cos^2(2\theta_2)}$

depending only on the Poisson's ratio of the soil ν_s.

$$\theta_{cr} = \cos^{-1}\frac{c_s}{c_p} = \cos^{-1}\sqrt{\frac{1-2\,\nu_s}{2\,(1-\nu_s)}} \tag{2}$$

If $\theta_o < \theta_{cr}$, the meaning of the reflected P wave has to be reviewed. The direction of propagation of this wave is given by eq. (3). Substitution of eq. (3) into the general expression of the displacements of the reflected P wave given by eq. (4), allows to obtain, after performing some transformations, the alternative expression shown in eq. (5).

$$\cos(\theta_2) = \frac{1}{\kappa}\cos(\theta_o)\,; \qquad \sin(\theta_2) = -\mathrm{i}\sqrt{-1+\frac{1}{\kappa^2}\cos^2(\theta_o)} \tag{3}$$

$$\begin{bmatrix} u_2 \\ u_3 \end{bmatrix}^P = \begin{bmatrix} \cos(\theta_2) \\ -\sin(\theta_2) \end{bmatrix} A_{\mathrm{p}}^{\mathrm{ref}}\, \mathrm{e}^{-\mathrm{i}\,k_p\,[\cos(\theta_2)\,x_2 - \sin(\theta_2)\,x_3]} \tag{4}$$

$$\begin{bmatrix} u_2 \\ u_3 \end{bmatrix}^P = \begin{bmatrix} \cos(\theta_o)/\kappa \\ \mathrm{i}\sqrt{-1+\cos^2(\theta_o)/\kappa^2} \end{bmatrix} A_{\mathrm{p}}^{\mathrm{ref}}\, \mathrm{e}^{\xi\,x_3}\, \mathrm{e}^{-\mathrm{i}\,k_s\,\cos(\theta_o)\,x_2} \tag{5}$$

with ξ being a real constant given by

$$\xi = +k_p\sqrt{-1+\frac{1}{\kappa^2}\cos^2(\theta_o)} \tag{6}$$

Eq. (5) corresponds to a wave that propagates horizontally, in the x_2 direction, with a velocity that depends on the angle of the incident SV wave. Such a wave produces horizontal

and vertical out–of–phase motions (u_2 and u_3) with an amplitude decreasing with depth, being this the reason why the sign of the square root in eq. (3) must be negative. Note also that, as $A_{\mathrm{p}}^{\mathrm{inc}}$ is a complex quantity, this wave is not necessarily in phase with the incident SV wave. Therefore, this reflected wave can be understood as a surface wave, influencing the dynamic response of structures submitted to the incidence of SV waves with angles of incidence below the critical one, as will be shown later.

3 Problem statement

3.1 Problem definition

This paper is focused on the analysis of the influence of the angle of incidence and type of wave on the dynamic response of piled structures. The problem is sketched in figure 2. For the sake of simplicity, the superstructure is studied as a single rigid slab supported by massless flexible and inextensible columns, and founded on a square pile group excited by SH, SV or P waves travelling in the x_2–x_3 plane, as shown in figure 2 and according to the coordinate system defined in section 2. This model of the superstructure can represent both a single–degree–of–freedom system (like a one–storey shear building) or an equivalent system defining the behaviour of a multimodal structure oscillating according to a specific mode of vibration.

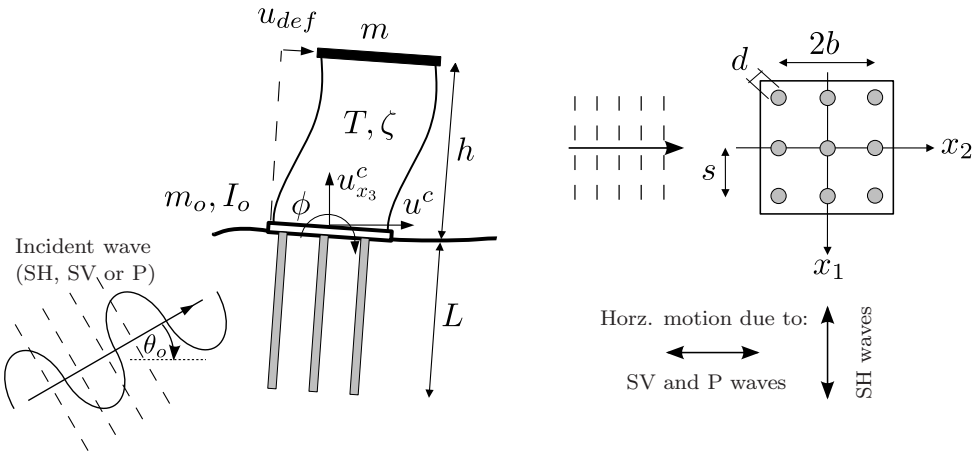

Figure 2: Problem definition.

The dynamic response of the structure can be defined by its rigid base fundamental period T, the height h of the resultant of the inertia forces for the mode under study, the mass m participating on the mode and the corresponding structural damping ζ. The horizontal stiffness of the structure is $k = 4\,\pi^2\,m/T^2$, with a hysteretic damping given by a complex stiffness of the type $K = k\,(1 + 2\,\mathrm{i}\,\zeta)$. The structure is founded on a 3×3 square pile group embedded in a viscoelastic halfspace. Pile groups are defined by the length L and diameter d of the piles, the centre–to–centre spacing s between adjacent piles, the pile cap mass m_o, its moment of inertia with respect to a horizontal axis going through its center of gravity I_o and by a parameter b measuring half of the width of the foundation.

If soil–structure interaction effects are taken into account, the behaviour of both the pile cap and the superstructure can be defined by that of a four–degree–of–freedom system. These degrees of freedom represent horizontal, vertical and rocking movements at the rigid pile cap (u^c, $u^c_{x_3}$ and ϕ, respectively) and inter–storey drift of the superstructure (u_{def}). Note that, as the columns are inextensible, rocking motion of pile cap and slab are identical.

3.2 Physical properties of the system

The geometric and material properties of the piles are: diameter $d = 1\,\mathrm{m}$, Young's modulus $E_p = 2.2 \cdot 10^{10}\ \mathrm{N\ m^{-2}}$, Poisson's ratio $\nu_p = 0.25$ and density $\rho_p = 2500\ \mathrm{kg\ m^{-3}}$. These values can be considered as typical for reinforced concrete. The soil properties are: Young's modulus $E_s = 2.2 \cdot 10^8\ \mathrm{N\ m^{-2}}$, Poisson's ratio $\nu_s = 0.4$, critical angle 65.9° and density $\rho_s = 1750\ \mathrm{kg\ m^{-3}}$.

With these properties, a velocity of the S waves in the soil of $c_s = 210$ m s^{-1} is obtained. Structural (ζ) and soil (β) damping ratios are equal and have a value of 0.05.

The previous values give rise to the following mechanical and geometric dimensionless relations both for soil and foundation: Young's modulus ratio $E_p/E_s = 10^2$, soil–pile densities ratio $\rho_s/\rho_p = 0.7$, and slenderness ratio of the piles $L/d = 15$. Besides, a ratio between pile separation and diameter $s/d = 5$ is used when studying the 3×3 piled foundation.

Two different configurations have been considered for the superstructure, a first one with a period of 0.159 s in which the vibrating mass, of $3.5 \cdot 10^5$ kg, is located at a height of 10 m and the mass and moment of inertia of the foundations are $8.75 \cdot 10^4$ kg and $1.75 \cdot 10^6$ kg m^2, respectively; and a second configuration with a period of 0.317 s, a vibrating mass of $7 \cdot 10^5$ kg at a height of 20 m, being the mass of the foundation $1.75 \cdot 10^5$ kg and its moment of inertia $1.4 \cdot 10^7$ kg m^2.

The preceding values lead to aspect ratios $h/b = 2$ and 4, to a ratio between the stiffnesses of structure and soil $h/(T\,c_s) = 0.3$, to a structure–soil mass ratio $m/\left(4\,\rho_s\,b^2\,h\right) = 0.2$ and to a foundation–structure mass ratio $m_o/m = 0.25$. The values chosen for the last three parameters are considered to be representative of typical constructions (see, e.g., [10, 11, 12]). In addition, the moment of inertia of the foundation is characterised by the 5% of the $m\,h^2$ factor.

4 Methodology

4.1 Numerical tool

In this work, a frecuency–domain boundary element–finite element formulation [13] is used to tackle the problem, being the Boundary Element Method (BEM) employed to model the soil as a homogeneous, isotropic, viscoelastic, semi–infinite region and the Finite Element Method (FEM) used to model piles as Euler–Bernoulli beams and superstructures as multi–storey buildings composed of vertical columns and horizontal rigid slabs. The system of equations arising from the application of the BEM to the soil is coupled with that resulting from using the FEM to model the motion of pile groups and superstructures, leading to a single system of equations describing the behaviour of the entire problem.

The loads acting in the problem consist of harmonic plane wavefronts propagating through the soil. The validity of the equations of the BEM–FEM model forces these expressions to be written in terms of the field diffracted by the foundation and by the structure. Putting this diffracted field as the difference between the total and the incident fields [14], the equations of the coupled model in terms of the former for every domain Ω (see [13]) can be expressed as:

$$H^{ss}\,u^s - G^{ss}\,p^s - \sum_{j=1}^{n_p} G^{sp_j}\,q^{s_j} + \sum_{j=1}^{n_p} \Upsilon^{sj}\,F_{p_j} = H^{ss}\,u_I^s - G^{ss}\,p_I^s \tag{7}$$

being H^{ss}, G^{ss} and G^{sp_j} the influence coefficients, u^s and p^s the displacements and tractions of the total field, n_p the number of piles in the domain, q^{s_j} the tractions along the pile–soil interface, Υ^{sj} a three–component vector representing the contribution of the axial force F_{p_j} at the tip of the j^{th} load line, and u_I^s and p_I^s the displacements and tractions of the incident field, which can be found using formulae described in section 2. This way, the right hand side of eq. (7) is known.

4.2 Definition of the input seismic motions

The input to the system is given by free–surface horizontal accelerograms generated making use of *SIMQKE* [15] to be compatible with a specific elastic response spectrum. In this work, the elastic response spectrum is taken from Part 1 of Eurocode 8 [7]. According to the system properties, a type 1 elastic response spectrum for ground type C and 5% damping is used. In order to achieve statistical significance, a set of three non–correlated accelerograms, with base–lines corrected according to [16], is used in this work. The magnitude of the design ground acceleration in terms of reference peak ground acceleration is $a_g = 0.25$ g (with peak ground acceleration for ground type C PGA $= 0.288$ g) and a duration of $t = 30$ s. A general incident field as that described in section 2 will originate, with the exception of the SH case, not only horizontal

but also vertical displacements at the reference point in the free surface. Therefore, the horizontal accelerogram described above will be associated, in general, with a vertical component. In the case of incident SV waves, the vertical peak ground acceleration (PGA_v) corresponding to the different angles of incidence is shown in Table 2 for $\nu = 0.4$. Note that, for $\theta = 57.7°$, the relationships between vertical and horizontal excitations would be in the order of the value recommended in Eurocode 8 [7] when defining a realistic vertical elastic response. On the other hand, for incident P waves, the corresponding vertical peak ground acceleration values would range from $\mathrm{PGA}_v = 0.563\,\mathrm{g}$ for $\theta_o = 55°$, to $\mathrm{PGA}_v = 2.015\,\mathrm{g}$ for the almost vertical $\theta_o = 80°$.

Table 2: Vertical peak ground acceleration (PGA_v) corresponding to different angles of SV incident waves. $\nu = 0.4$. Horizontal PGA$= 0.288\,\mathrm{g}$.

angle (°)	90	80	70	66	$\theta_{cr} = 65.9$	65	60	57.5	55
PGA_v (g)	0	0.040	0.058	0.012	0	0.040	0.167	0.256	0.389

4.3 Computation of time–history results

The abovementioned BEM–FEM numerical model can be used to obtain the frequency response functions relating different magnitudes of interest, such as bending moments or lateral deflections, to the seismic excitation.

The following section of this article shows several results obtained from the estimation of time–history moments at pile heads. These values in time domain of the bending moments are calculated by taking the inverse Fourier transform of the product $H(\omega)\, X(\omega)$, where $X(\omega)$ is the Fourier transform of the free–field horizontal accelerations at ground surface used to define the excitation. Thus, $H(\omega)$ has to be defined as the ratio between the bending moments ($M(\omega)$) and the free–field horizontal accelerations at ground surface ($\ddot{u}_{ff}(\omega)$) at point $(0,0,0)$. Therefore, it is of interest to analyse the evolution of the factor $|u_{ff}|/A^{\mathrm{inc}}$ with the angle of incidence (i.e., with θ_o) since $H(\omega)$ will strongly depend on it. Figure 3 shows the variation of this factor for different values of the Poisson's ratio of the soil. It can be seen that the free–field displacements are independent of the angle of incidence for SH waves, while the variation is smooth and dependent on the Poisson's ratio of the soil for P waves. However, a different trend is observed in SV waves. The displacements observed for angles comprised between 0 and 50 degrees are significantly smaller than those corresponding to more vertical incident waves, although the variation is smooth in the range between 0 and 45 degrees (with null values of the displacement for such angles). This produces the SV frequency response functions, once normalised by the free–field horizontal displacements, to have values of different orders of magnitude for angles of incidence smaller or greater than about 50°. Even more, the frequency response functions will not be defined for 45° since $|u_{ff}(\theta_o = 45°)|/A^{\mathrm{inc}}_{\mathrm{SV}} = 0$.

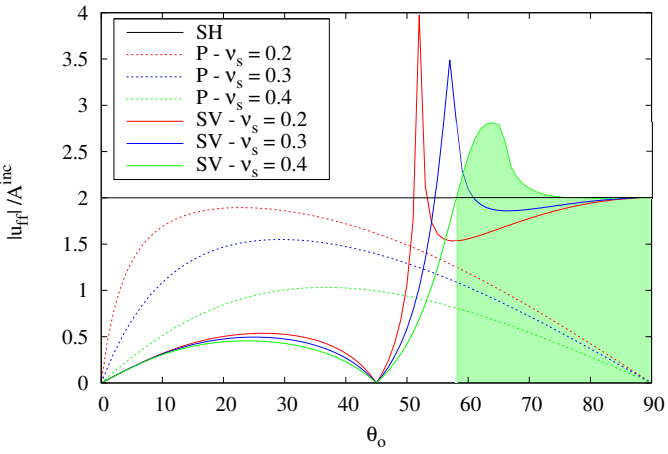

Figure 3: Variation of the modulus of the free–field horizontal displacement with the angle of incidence in the plane $x_2\, x_3$ for SH, P and SV incident wavefronts. The green shadow represents the selected range of angles of incidence for the chosen value of $\nu_s = 0.4$.

On the other hand, actual soils are seldom homogeneous. On the contrary, they are usually layered, with the stiffness of the strata increasing with depth. For this reason, it is generally assumed that the probability of arrival to the surface of significantly non–vertical incident S or P plane waves is reduced because of the processes of refraction that take place in the interfaces. Therefore, in order to make the results for obliquely incident waves relatively comparable, only angles of incidence comprised between 55 and 90 degrees (zone defined by a green shadow in figure 3) will be considered from this point forward.

4.4 Validation of the BEM-FEM Code

The aim of this subsection is the validation of the proposed formulation through a set of comparison results. First, kinematic interaction factors, in terms of displacements and rotations, are presented against those previously published by Kaynia & Novak [5]. The properties of piles and pile groups are: $E_p/E_s = 100$, $\rho_p/\rho_s = 1.5$, $\beta = 0.05$, $L/d = 20$, $\nu_p = 0.25$, $\nu_s = 1/3$ and $s/d = 5$. Figure 4 shows the comparison for single piles and 3×3 pile groups under incident SV waves, while figure 5 shows the case of single piles and 4×4 pile groups under incident P waves. In both cases, a very good agreement is reached.

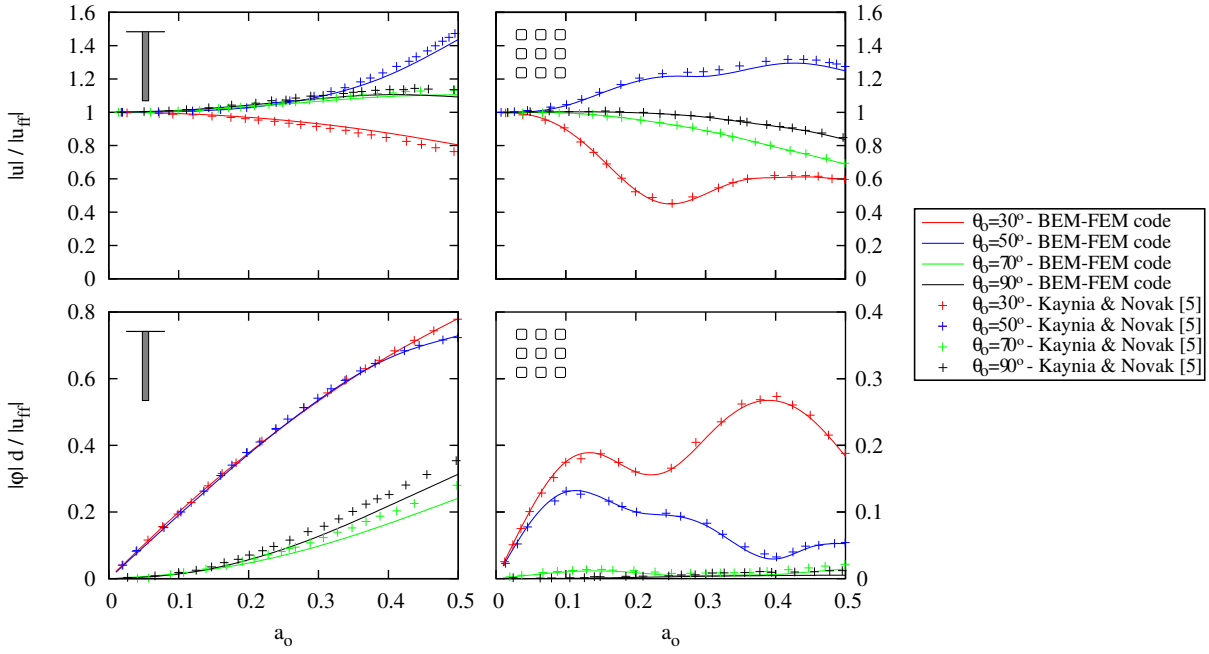

Figure 4: Absolute value of the frequency response functions for horizontal displacements (top) and rocking (bottom) of single piles (left) and 3×3 pile groups (right) under SV incident waves. Comparison against results by Kaynia & Novak [5].

In second place, the frequency response functions for the bending moments at the pile head for a single pile problem are presented both by the BEM-FEM coupled model and by multidomain BEM model [17]. The main properties of the problem are: $E_p/E_s = 100$, $\rho_s/\rho_p = 0.7$, $L/d = 20$, $\beta = 0.05$, $\nu_p = 0.25$ and $\nu_s = 0.4$. Rotation and vertical displacement at pile head are not allowed whereas horizontal displacement is permitted. The results are represented in figures 6 and 7 for different angles of incidence (θ_o) of an impinging SV wavefront. In figure 6, real and imaginary parts of the bending moments at the pile head, presented in a dimensionless form, are shown against the dimensionless frequency (defined as $a_o = \omega\, d/c_s$) for three angles of incidence more vertical than the critical one. These dimensionless moments are obtained dividing the bending moments by the free–field horizontal displacement and by a cross–coupled term of the stiffness of an Euler–Bernoulli beam, linked to the relationship between displacements at one end of the beam with the bending moments developed in such a point. More precisely, and despite several other angles have been compared, results for 90, 75 and 60 degrees are shown for the sake of brevity. In addition, figure 7 presents results for angles of incidence around the critical one (i.e., for 65, 65.8 and 66 degrees, being the critical angle $\theta_{cr} = 65.9°$). A very good agreement between both methodologies can be seen, especially in the low–frequency range, with

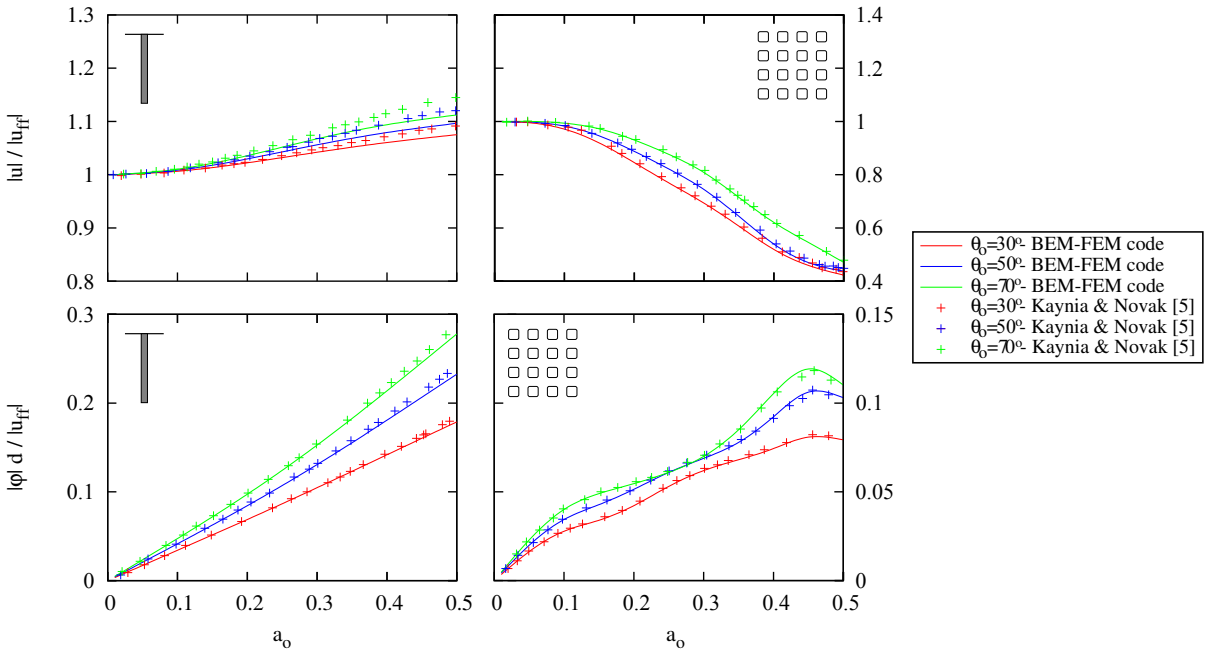

Figure 5: Absolute value of the frequency response functions for horizontal displacements (top) and rocking (bottom) of single piles (left) and 4×4 pile groups (right) under P incident waves. Comparison against results by Kaynia & Novak [5].

maximum errors up to a 10%. Once the BEM–FEM model has been proven to be a valid tool for this problem, and taking into consideration that this approach is far less costly than the more rigorous BEM–BEM one and, as a consequence, allows to perform parametric analyses easier, such a tool will be used from now on.

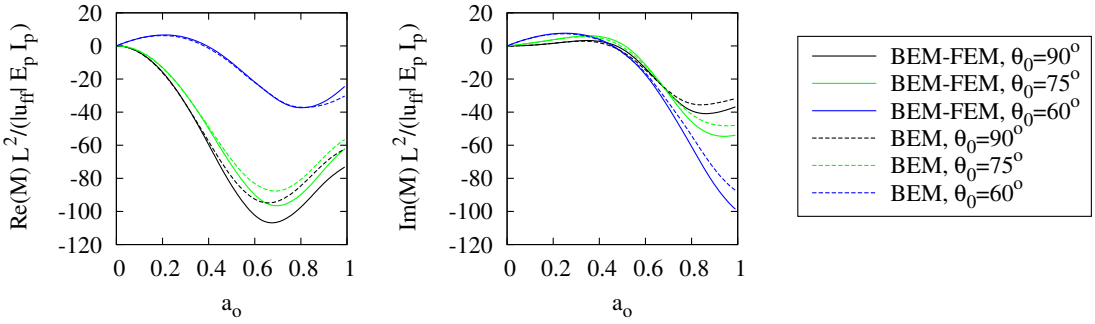

Figure 6: Real and imaginary parts of the transfer functions of the bending moment at the single pile head. Incident SV waves. 90, 75 and 60 degrees.

5 Results

5.1 Influence of angle of incidence on bending moments at single pile heads

In order to discern the general trends and the most interesting features of the problem at hand, this section addresses again the seismic response, in terms of bending moments at the pile head, of a single pile embedded in a halfspace. The main properties, boundary conditions at the pile head and type of incident wave (SV wave) are the same that were used in the previous section 4.4. Since the influence of pile-to-pile interaction on the kinematic response of pile groups for a vertically-incident wavefield is small in the low and intermediate frequency ranges [18], this problem constitutes a good first approach. This way, a parametric analysis is performed on this simpler problem to investigate the influence of type of wave and angle of incidence on the seismic response of the system. The conclusions drawn from this study will be useful for interpretation of the results corresponding to a pile group.

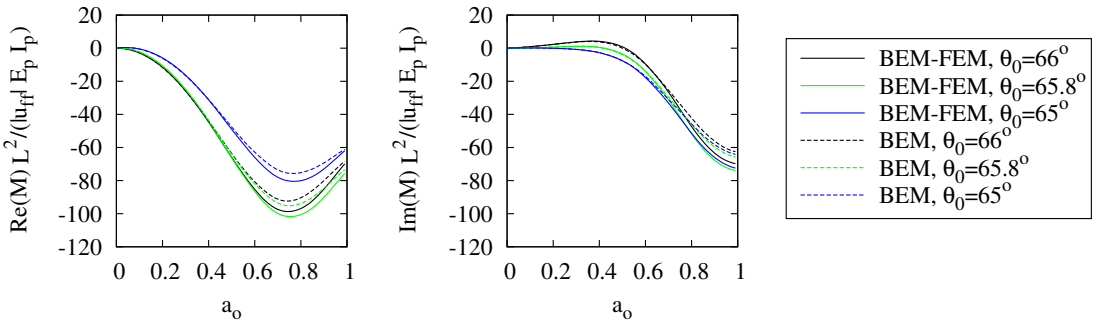

Figure 7: Real and imaginary parts of the transfer functions of the bending moment at the single pile head. Incident SV waves. Angles around the critical one (66, 65.8 and 65 degrees, $\theta_{cr} = 65.9°$).

5.1.1 Frequency response functions

Figure 8a represents the values of the modulus of the dimensionless bending moment for a discrete set of dimensionless frequencies ($a_o = 0.01$, 0.05, 0.1, 0.2, 0.3 and 0.4) against the angle of incidence. Results are obtained for angles between 55 and 90 degrees in steps of 2.5° with additional values around the critical angle (65.8, 66 and 67 degrees). An inflection point can be seen for $\theta_o = \theta_{cr}$, which can be understood taking into account the change in the mechanism of propagation of the waves in the soil produced in such an angle. Below this angle, the variability of the bending moments is much greater than after it, where the moments notably increase with θ_o and a_o.

An alternative representation of figure 8a is shown in figure 8b, where the frequency response functions for the bending moment at the pile head are plotted against the dimensionless frequency for a set of angles of incidence (55, 60, 65, 65.8, 66, 70, 80 and 90 degrees). It is seen that the trends are similar for all the angles with the exception of 55 and 60 degrees. The tendencies for these two angles can be explained taking into account that the surface waves that appear for angles of incidence smaller than the critical one produce, in the points located close to the surface, free–field displacements that vary notably with the angle of incidence. This way, and depending on the angle of incidence and on the frequency of excitation, such incident field can tend to increase or reduce the internal efforts at the pile head, which gives rise to the different behaviours observed in the figure.

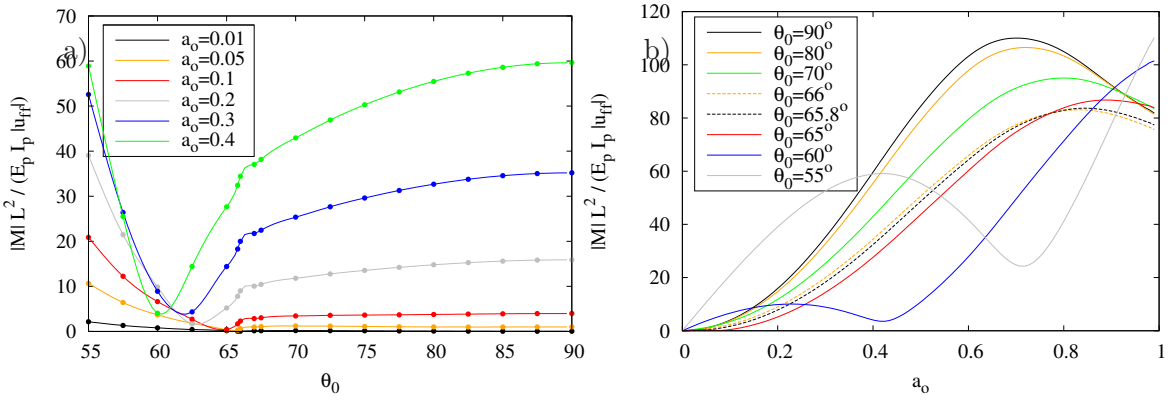

Figure 8: Dimensionless moduli of the bending moment at the single pile head. Incident SV waves. Angles of incidence between 55 and 90 degrees.

5.1.2 Envelopes of the maximum bending moments for synthetic accelerograms

Figure 9 presents the evolution of the envelopes of the maximum bending moments developed at the pile head with the angle of the incident SV wave when the system is subjected to the three accelerograms defined in section 4.1. The maximum value of the bending moment is obtained for an angle of incidence of 55°. As the incidence of the waves becomes more vertical, the moments

sharply decrease until they reach a minimum value around the critical angle. Then, this value nearly duplicates for 70°, gently decreasing between a 10 and a 30%, depending on the input accelerogram, with the angle of incidence from such an angle onwards. It is also shown that the results are very similar with independence of the accelerogram used to define the free–field horizontal accelerations.

To have a reference of the magnitude of the obtained values, the maximum moment resisted by the section of the pile for a variable value of the axial load, calculated using the interaction diagrams of [19], according to Eurocode 2 [20], is represented by means of a grey band. It is then necessary to define the materials, the reinforcing bars used in the section and the range of axial loads considered in the study. Using a concrete of class C 25/30 reinforced with 10 bars of steel of class S 500 of 25 millimetres of diameter, a maximum moment comprised between $8.5 \cdot 10^5$ N m and $9.8 \cdot 10^5$ N m is resisted by the section of the pile when the axial load varies between 0 and 500 kN. Considering these values, figure 9 shows the relevance of the angle of incidence on the dynamic response of the analysed pile foundation, since it can be seen that the maximum moment resisted by the section of the pile can be reached for an angle of incidence of 55°, while it is much smaller below such critical value for vertical incidence. Note that the bending moments presented in figure 9 are only due to the effect of the kinematic interaction. To see the evolution of the system response in detail, figure 9 shows, in its bottom row, a zoomed version of the values.

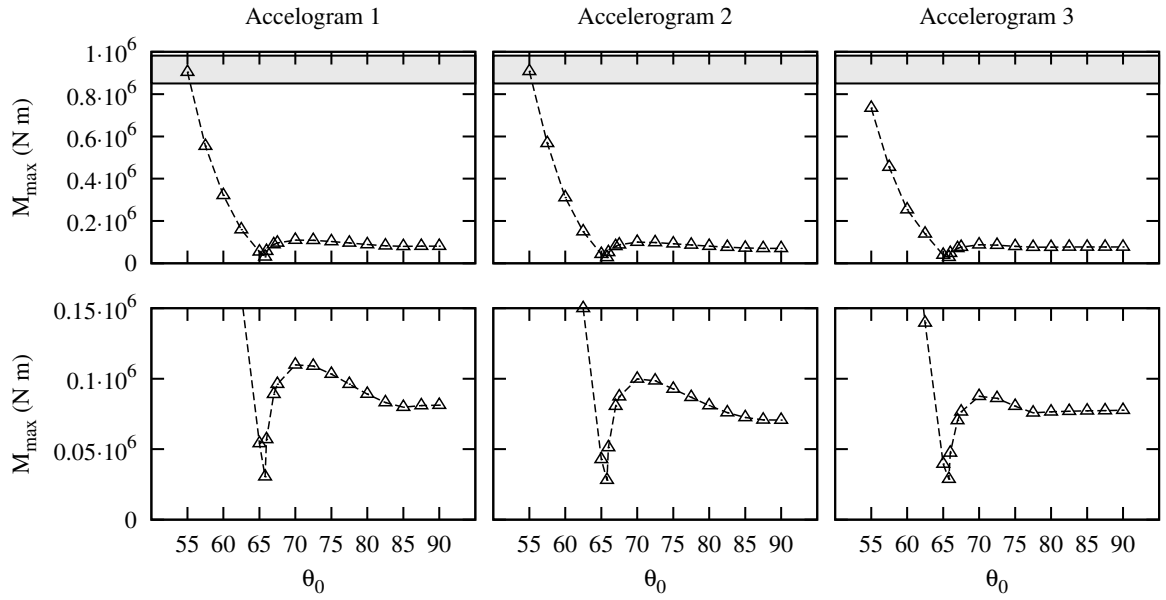

Figure 9: Envelopes of maximum bending moments for the single pile problem. Incident SV waves. Angles of incidence between 55 and 90 degrees. A zoomed version of values in top row can be seen in the bottom row. The grey zone represents the maximum moment resisted by the section of the concrete pile with C25/30 reinforced with 10∅25mm steel bars.

5.2 Influence of the angle of incidence and type of seismic wave on bending moments at heads of piles in a group

The problem presented in the previous section was used to highlight the influence of the angle of incidence on the dynamic response of a single foundation. This section will look into the response of pile groups to obliquely–incident seismic waves to highlight the importance of pile–to–pile interaction. To this end, the response of the 3×3 pile foundation described in section 3 will be studied. The influence of inertial interaction will also be studied by considering a single–degree–of–freedom system founded on the pile foundation. Results will be obtained for three different configurations. The first one considers exclusively the effect of kinematic interaction whereas the second and the third configurations take into account both the kinematic and the inertial effects, differing in the aspect ratio h/b of the superstructure.

5.2.1 Frequency response functions

The first set of results presents a selection of frequency response functions for the bending moment at pile heads. Results are shown for a dimensionless frequency range between 0 and 0.4 because it is the most interesting one from the seismic analysis point of view. However, the trends seen in figure 8 for the single pile are indicative of the behaviour of the systems at higher frequencies.

Figure 10 presents the transfer functions for the problem involving incident SV waves with angles ranging from 55 to 90 degrees when only the kinematic interaction is taken into account. The small plot at the top left of the figures represents the nine piles of the group, where the shadowed one indicates the one being analysed. For comparison purposes, results for a single pile with the same L/d slenderness ratio are presented in the top right corner of the figure.

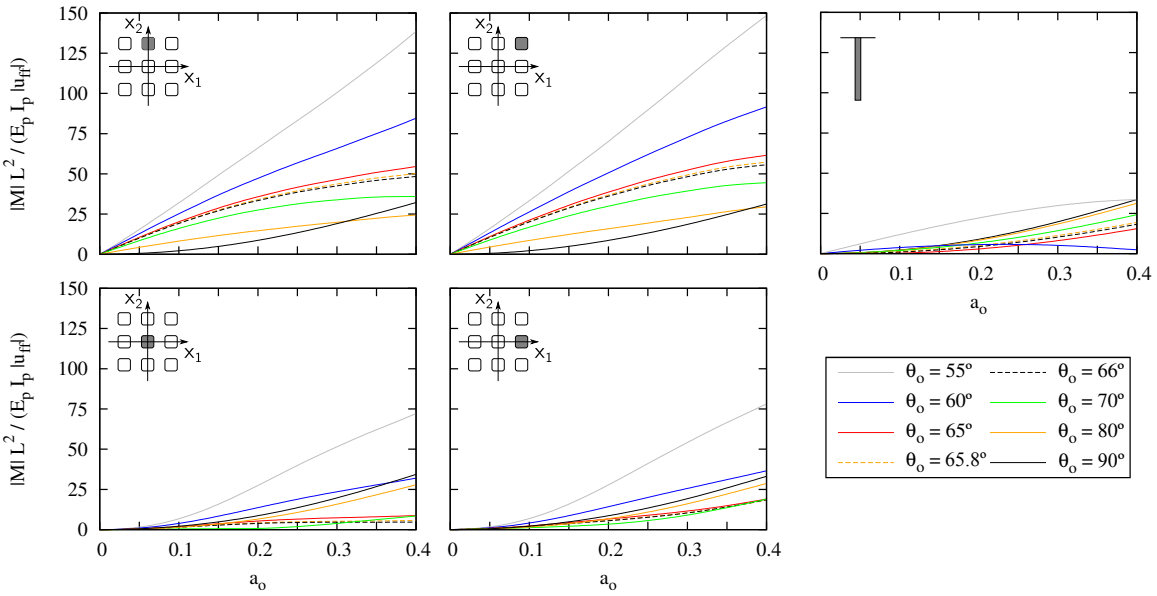

Figure 10: Frequency response functions for the bending moment at pile heads. 3×3 pile group. Kinematic interaction. Incident SV waves. Angles of incidence between 55 and 90 degrees.

In the frequency range of interest, translational kinematic interaction factors for vertically–incident waves have been shown to be almost independent of the number and configuration of the piles [18]. Pile–to–pile interaction is also of very little importance when looking at the internal efforts of piles in groups subjected to vertically–incident S waves [21]. This way, figure 10 shows that, for $\theta_o = 90°$, the bending moments are very similar in all cases, i.e., among all piles in the group and also with respect to the single pile with no rotation at the head, which is consistent with [18]. However, this trend does not hold for non–vertical incidence, as the response varies strongly among piles in the group and also with respect to the single pile.

In this regard, relevant differences between the frequency response functions for the bending moments for single piles and for the pile group (figure 10) are noticed. The different behaviours can be explained analysing the variability of the incident field displacements in the direction of propagation of the non–vertical waves. In this case, the incident field is such that points placed at the same depth but close to different piles in a group can be experiencing, at a given time, different displacements, in some cases even of opposite signs. These differences increase with frequency and are also more important for angles of incidence smaller than the critical one, when surface waves come into play. When the presence of the pile group is taken into account, the kinematic restriction imposed by the pile cap prevents the piles to move independently and, as a consequence of the phase lag, displacements corresponding to pile groups are significantly smaller than those of a single pile, and bending moments at pile heads in a group notably increase in comparison to the single pile case.

Figure 11 shows, for an SV incident wave propagating with an angle of 60° and for $a_o = 0.4$, a comparison between the free–field displacements in different x_2 coordinates (note that the incident waves propagate in the $x_2\,x_3$ plane along the positive x_2 direction) corresponding to the position of a certain pile, and the deformed shape of such a pile. The top row of the figure

represents the real part of the displacements, while the bottom row presents their imaginary part. The first column refers to the single pile problem (located at $x_2 = 0$) while the other two show results for the problem involving a pile group, where two piles, the central and the top ones located at $x_2 = 0$ and $x_2 = 5\,d$, are studied. The single pile is capable of following the free–field displacements, while piles belonging to the group cannot. The difference between the displacements in the soil due to the incident field and the deformed shape of every pile is much higher in the outer ones because of the kinematic compatibility imposed by the rigid cap, and it is precisely for this compatibility that piles in the group develop higher moments than those developed in the case of single piles for non–vertical incidence. Also, pile–soil interaction forces will be much higher in the case of the pile group as they are proportional to the difference between the displacements in the soil due to the incident field and the deformed shape of the pile.

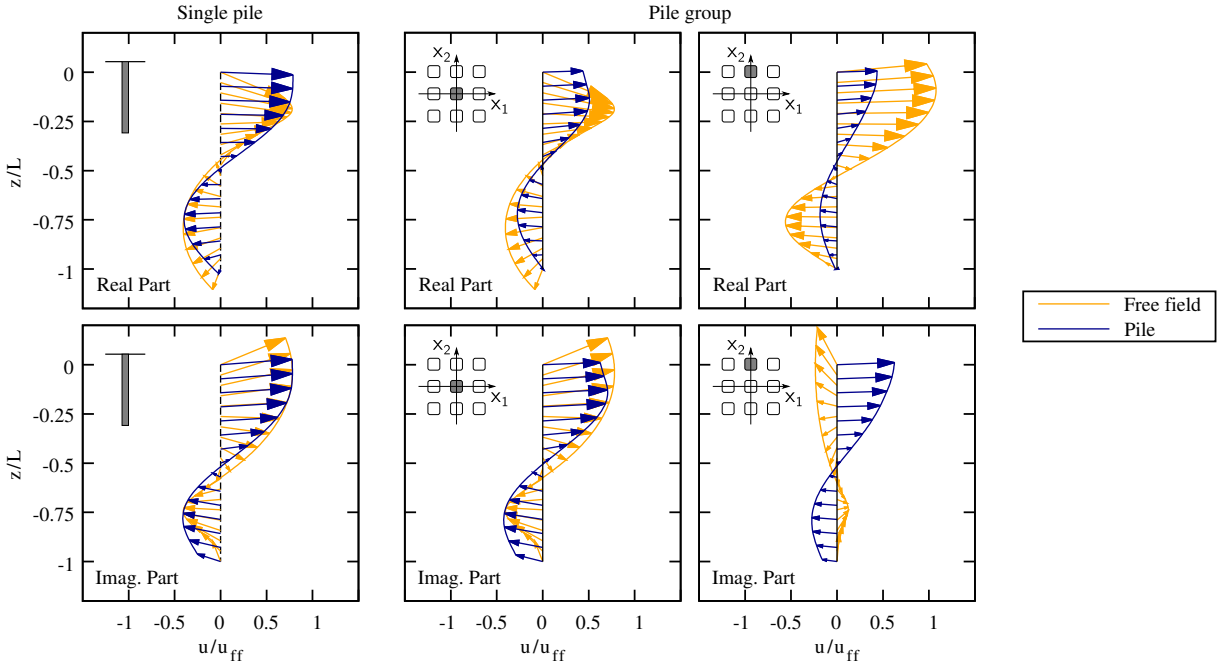

Figure 11: Comparison between real (top row) and imaginary (bottom row) parts of the free–field displacements and the corresponding pile deformed shape. Single pile (left) and pile group (center and right). Incident SV waves. Angle of incidence of 60°. $a_o = 0.4$.

Returning to the presentation of the frequency response functions of the pile group, figure 12 plots the bending moments at pile heads for such a problem, this time taking into account the presence of a superstructure with an aspect ratio of $h/b = 2$. The results show a peak around the flexible–base fundamental frequency of the system (around a dimensionless frequency of 0.14). Once again, the maximum moments are obtained for an angle of incidence of 55°. Small differences are seen in comparison with the problem including only the effects of kinematic interaction, and only around the fundamental frequency of the superstructure. The resonance arising around such frequency can produce both increments or decrements of the bending moments depending on the angle of incidence and on the location of the pile, being this a phenomenon that cannot be explained by the authors at the moment, and which should be further studied.

The frequency response functions corresponding to the piles in a group supporting a superstructure with an $h/b = 4$ aspect ratio are represented in figure 13. The flexible–base fundamental frequency of the system is now around a dimensionless frequency of 0.08. The frequency response functions shown in figures 10, 12, and 13 are all very similar, being the differences located mainly around the fundamental frequency of the soil–structure system only. Therefore, in these cases, and under incident SV waves, moments at the pile heads produced by kinematic interaction are of much higher importance that those produced by inertial interaction with the superstructure. It will be shown below that this relative importance between moments produced by kinematic or inertial interaction also depends on the type of incident wave.

Figure 14 presents the frequency response functions for the bending moment at the head of

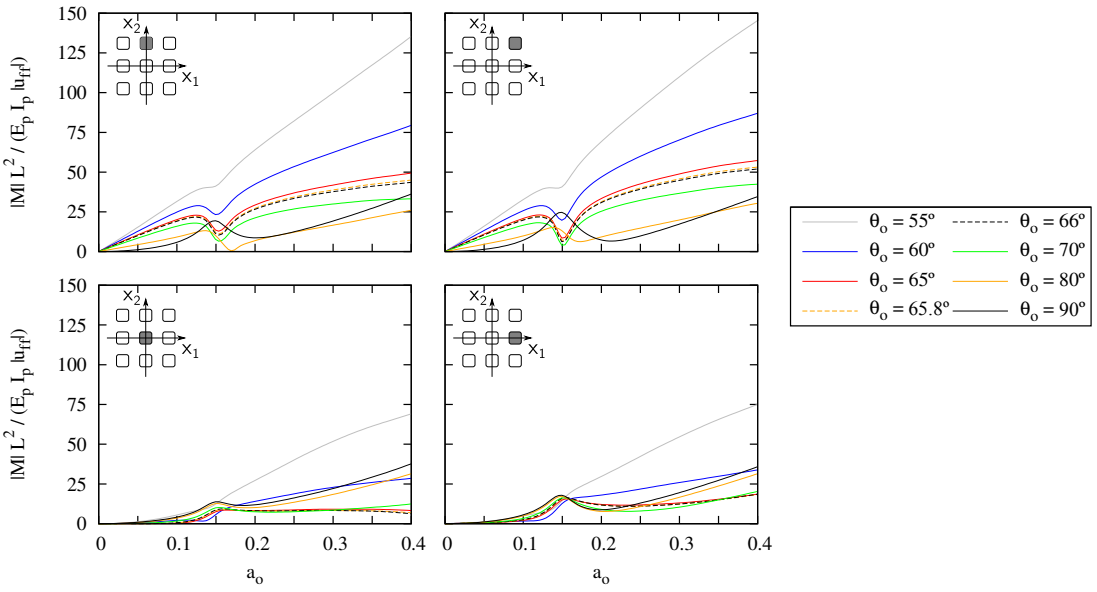

Figure 12: Frequency response functions for the bending moment at pile heads. 3×3 pile group. $h/b = 2$. Incident SV waves. Angles of incidence between 55 and 90 degrees.

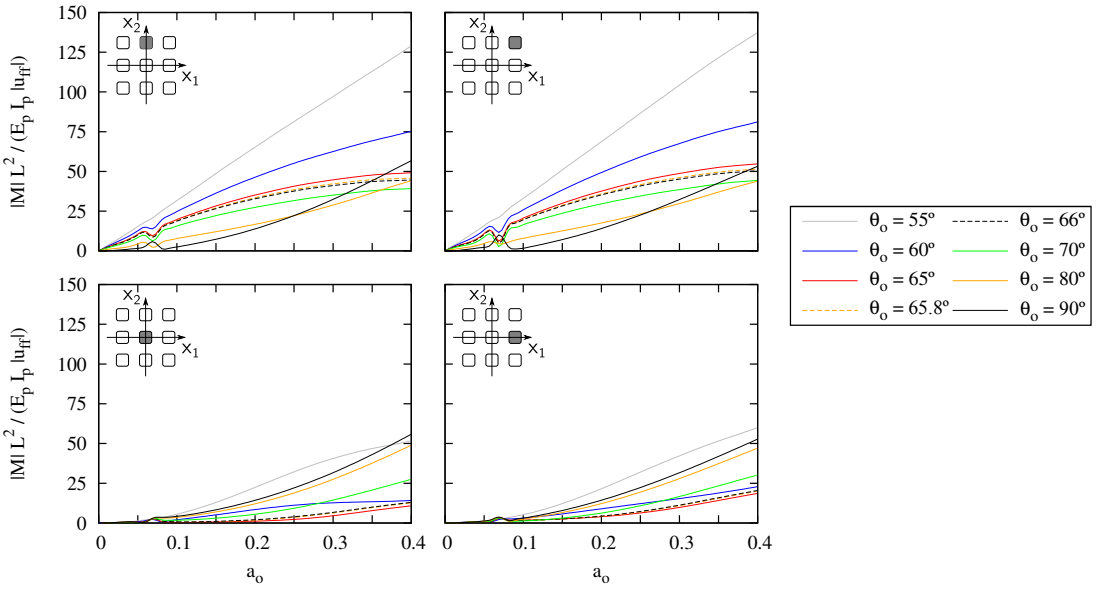

Figure 13: Frequency response functions for the bending moment at pile heads. 3×3 pile group. $h/b = 4$. Incident SV waves. Angles of incidence between 55 and 90 degrees.

the corner pile of the group (top plot) and at the head of the lateral pile of the group (bottom plot) for incident SH waves with angles of incidence between 55 and 90 degrees. Three columns are presented in this and in the following figures: the first one represents the problem taking only into account the effect of kinematic interaction, while the second and third columns present the results for $h/b = 2$ and 4, respectively. The results present a very similar tendency to that of incident SV waves, exhibiting resonance peaks around the fundamental frequency of the soil–structure system.

Note that the magnitude of the kinematic bending moments produced by the SH waves is much smaller than those produced by the incident SV waves. It is for this reason that inertial interaction, whose magnitude is expected to stay independent of the type of incident wave, has a bigger relative influence on the overall pile response when subjected to SH waves. In this case, the influence of the angle of incidence on the response of the central and top piles is of very reduced importance, contrarily to what happened in the case of incident SV waves. However, the same line of argument do not apply for the rest of piles, where important differences appear.

Note that the representation of the results corresponding to the top and central piles of the group have been omitted due to space considerations.

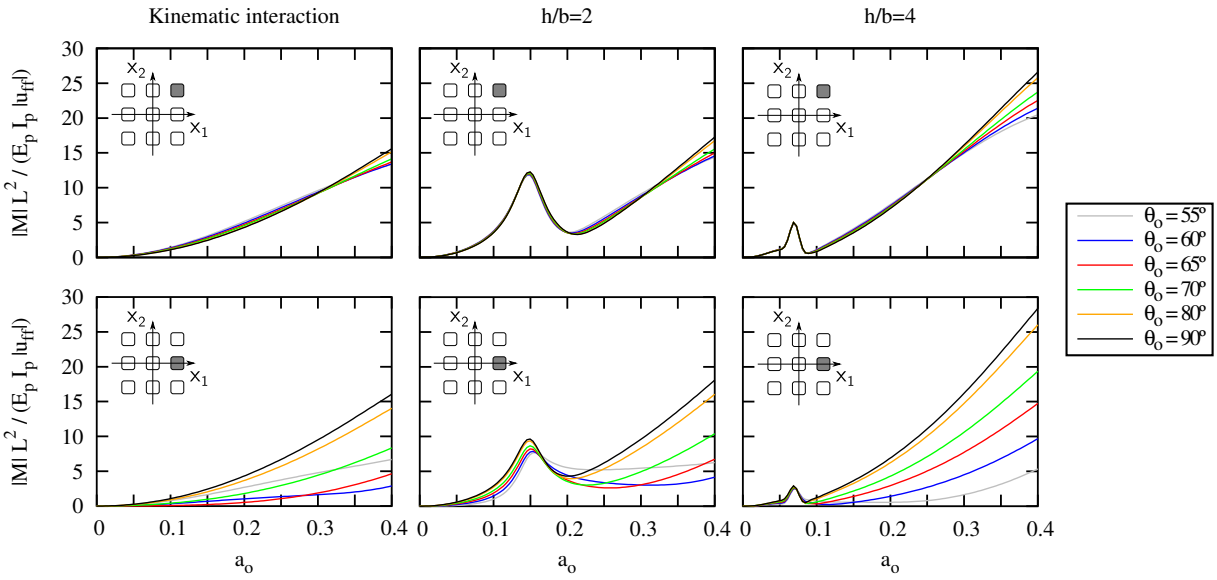

Figure 14: Frequency response functions for the bending moment at the head of the corner (top) and lateral (bottom) piles. 3×3 pile group. Incident SH waves. Angles of incidence between 55 and 90 degrees.

Figure 15 presents the frequency response functions for the bending moment at the head of the corner pile of the group for incident P waves with angles of incidence between 55 and 80 degrees. The influence of the angle of incidence on the bending moments increases with frequency and shows maximum values for an angle of incidence of 80°. Also, the influence of inertial interaction is reduced, as in previous cases, to the presence of a resonance peak around the natural frequency of the system. It is also interesting to note that, both for incident P and SH waves, the response at the pile heads in terms of bending moments is, for $55 < \theta_o < 70$ and $0 < a_o < 0.4$, less dependent on the angle of incidence than in the case of incident SV waves. However, for $a_o < 0.15$, the differences are significant in the case of P waves, especially in the outer piles of the group (not all shown), even though they cannot be appreciated in figure 15 because of the scale used in the representation of the results.

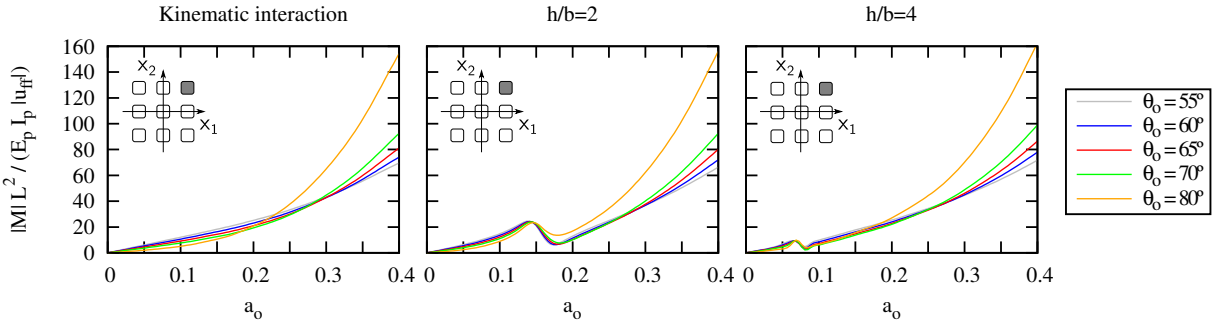

Figure 15: Frequency response functions for the bending moment at the head of the corner pile. 3×3 pile group. Incident P waves. Angles of incidence between 55 and 80 degrees.

5.2.2 Envelopes of the maximum bending moments for synthetic accelerograms

Results in time domain for the configurations and input motions defined in section 4 will now be shown. Figure 16 shows the envelopes of the maximum bending moments at pile heads for different angles of incident SV waves taking into account the three accelerograms defined in section 4 as inputs. Once the general tendencies of the results have been studied by means of the single pile problem, a fewer number of angles of incidence are computed, being the obtained

values marked with dots. Results are shown in two rows, being represented in the lower one a zoom of the general results corresponding to the inner piles in order to have a better view of their tendencies. As in the single pile case, the maximum moment resisted by a pile is presented by means of a set of grey bands. In this instance, three ranges of maximum moments resisted by the section of a pile made of C 25/30 reinforced concrete with three different amounts of reinforcement and subjected to an axial force variable between 0 and 500 kN are obtained [19] and represented. This way, the lower value corresponds to a reinforcement of 10 bars of S 500 steel of 25 millimetres of diameter, while the second one is obtained with 16 bars of S 500 steel of 32 millimetres and the higher value is reached with 26 bars of S 500 steel of 32 millimetres of diameter.

The shape of the envelopes is similar independently of the superstructure's aspect ratio. The tendency followed by the piles located in the inner side of the pile cap is the same than in the single pile, with a minimum around the critical angle. The magnitude of the bending moments in the outer piles is much greater than that developed in the inner piles of the group. Besides, the moment estimated in the outer piles varies almost linearly with the angle of incidence, with a maximum value for 55° and a minimum for vertical incidence. Finally, the effect associated with inertial interaction is more noticeable in the inner piles because the magnitude of the moments produced by kinematic interaction is much smaller, being constant the contribution of inertial interaction for all the piles of the group.

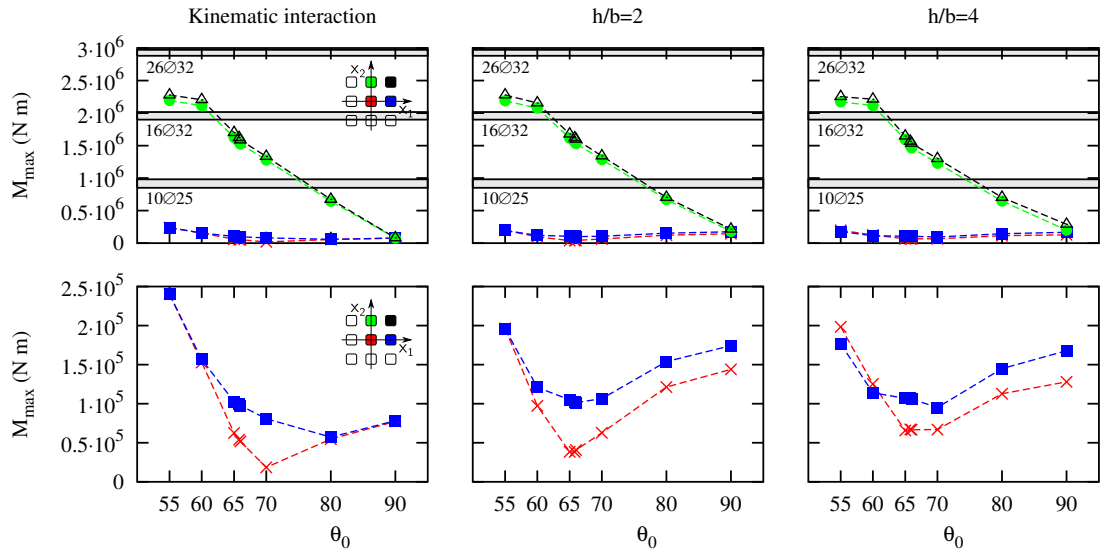

Figure 16: Envelopes of maximum bending moments. Incident SV waves. Angles of incidence between 55 and 90 degrees. The grey zones represent the maximum moment resisted by the section of the concrete pile with C25/30. Three diferent amounts of reinforcement (indicated in the graph) are used.

With regard to incident SH waves, the envelopes of maximum bending moments at pile heads, taking into account the three accelerograms defined in section 4, can be seen in figure 17. It is shown that the bending moments are nearly independent of the angle of incidence for the inner piles. For the outer piles, however, there is a significant variation with the angle of propagation of the incident wavefield. There are noticeable differences between the values developed only due to kinematic interaction and those arising from the problem including the building. As the magnitude of the bending moments due to the kinematic interaction is much smaller for SH than for SV waves, the influence of the superstructure becomes more apparent in this case. The absolute magnitude of the inertial interaction is expected to be approximately constant in every case, being this the reason why the influence of the superstructure is greater for SH waves only in relative terms. Besides, the higher dissimilarities that can be observed in the low–frequency range between the corresponding frequency response functions for incident SH waves can also explain the aforementioned differences between the values for kinematic interaction and for the problem including inertial interaction, since the time–history is dominated by the low frequencies. However, and with the only remarkable case of the pile located at the corner of the

group, there is no significant difference between the results obtained for an aspect ratio of 2 and those for a value of the aspect ratio of 4. In general terms, the efforts in the outer piles of the group (i.e., the green and the black piles) tend to decrease, up to about a 23%, as the angle of incidence becomes more vertical, while the opposite trend is verified for the inner piles (i.e., the red and the blue piles), with increments up to about a 268%. It is also worth pointing out that the results are much smaller than the corresponding values for the non–vertical incident SV waves.

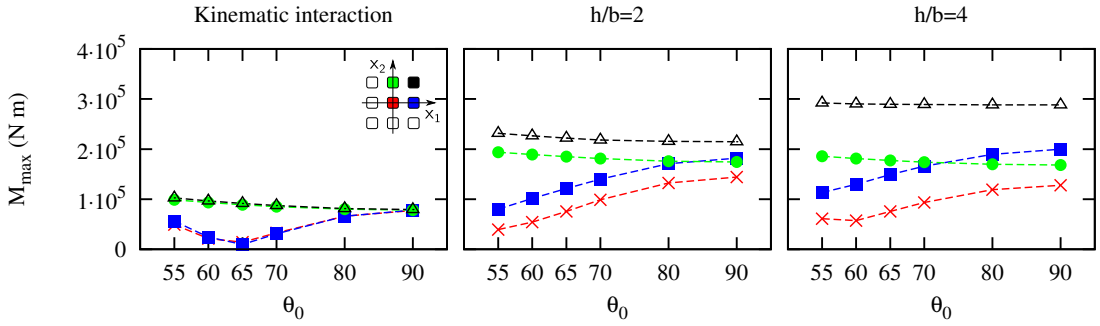

Figure 17: Envelopes of maximum bending moments. Incident SH waves. Angles of incidence between 55 and 90 degrees.

Finally, figure 18 shows the envelopes for incident P waves, considering the three accelerograms defined in section 4, where only the maximum values for each aspect ratio are presented anew. The results exhibit a very similar trend to those concerning incident SV waves. Summarising, the outer piles present similar values, decreasing nearly linearly with the angle of incidence, while the inner piles are submitted to almost the same value of the bending moment with independence of the angle of incidence. The magnitude of these moments is comprised between that of SV and SH incident waves, being lower than the former and higher than the latter. For this reason, the influence of the presence of the superstructure is, in this case, more noticeable than in the SV case, but less important than in the SH case.

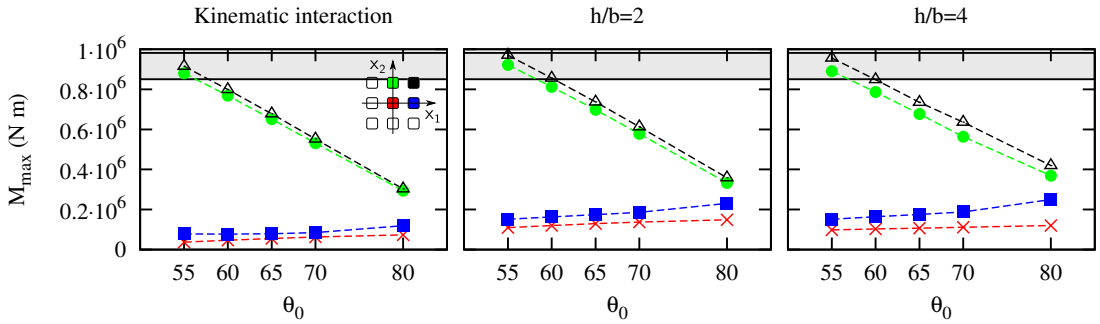

Figure 18: Envelopes of maximum bending moments. Incident P waves. Angles of incidence between 55 and 80 degrees. The grey zone represents the maximum moment resisted by the section of the concrete pile with C25/30 reinforced with 10∅25mm steel bars.

6 Conclusions

The influence of the type of incident seismic waves and of its angle of incidence on the dynamic response of pile foundations is investigated in this paper by means of a BEM–FEM coupled methodology. The formulation implemented for the study, the methodology used in the analyses, and the definition of the problem at hand are first briefly presented. Then, different configurations are studied. In order to highlight some basic features of the problem, the case of a single pile subjected to obliquely–incident SV waves is addressed in the first place. Afterwards, a 3×3 pile group subjected to SH, SV or P obliquely–incident waves is studied. Here,

not only the effect of kinematic interaction, but also that of the inertial interaction is analysed by considering the presence of a superstructure.

The most important conclusions that can be drawn from this study are:

- In the case of single piles subjected to SV waves, the largest bending moments arising at the pile heads does not necessarily occur for vertical incidence. In the frequency response functions, an inflection point can be seen at the critical angle due to the change in the mechanism of propagation of the waves in the soil produced at such an angle. For angles of incidence more horizontal than that, the variability of the bending moments with the angle of incidence is much larger than for more vertical angles, situation this last one in which bending moments increase with frequency and angle of incidence, being this increase more moderated at low frequencies.

- For low frequencies, the largest moments arise for angles of incidence more horizontal than the critical one. For this reason, the envelopes of bending moments in time domain for single piles subjected to synthetic accelerograms show that piles designed to withstand safely the bending moments developed under vertical incidence would fail for angles of incidence more horizontal than the critical one.

- The central piles of a group subjected to SV waves keep the trends observed in the frequency domain in the single pile, but the outer piles withstand much larger bending moments due to the kinematic restriction imposed by the rigid cap. Besides, the bending moments at the heads of these outer piles increase as the angle of incidence becomes more horizontal, both for SV and P incident waves. The kinematic bending moments are independent of pile–to–pile interaction only for vertical incidence.

- The envelopes of maximum bending moments in time domain for pile groups subjected to SV and P waves show trends similar to those already described above for the frequency domain. In this case, and contrarily to what happens for single or central piles, the maximum bending moments developed at the outer piles increase almost linearly as the angle of incidence becomes more horizontal.

- The maximum bending moments developed in time domain at the heads of piles in a group subjected to SH waves increase, as expected, with the presence of a superstructure. However, for the cases studied here, the large kinematic bending moments due to non–vertical P and SV waves imply a much smaller relative importance of the inertial interaction in the case of incident P waves, and an even smaller relative influence when SV waves are considered. Besides, for P and SV waves, the contribution of inertial interaction is more important in the central piles, where the kinematic bending moments are smaller. For SH waves, on the contrary, inertial interaction has similar effects on all piles in the group. When observing the frequency response functions, the effect of inertial interaction becomes significant only around the fundamental frequency of the system.

- In the case of incident SH waves, the presence and properties of a superstructure have a much larger effect on the frequency response functions for the bending moments than the angle of incidence. In fact, maximum bending moments in the outer piles are independent of the angle of incidence while, for central piles, bending moments are maximum for vertical incidence. On the contrary, for incident SV waves, the angle of incidence is the most important parameter.

As a summary, this paper highlights the importance of considering the characteristics of the seismic excitation when estimating the internal forces in pile foundations. In particular, this paper studies the influence of the type of wave and its angle of incidence on the estimation of the bending moments developed in the pile heads of deep foundations. The propagation of non–vertical waves, especially of obliquely–incident SV waves with angles of incidence smaller than the critical one, results in bending moments much larger than those obtained for vertically–incident wavefields. It has also been shown that the influence of pile–to–pile interaction on the kinematic bending moments at pile heads (insignificant for vertical incidence) increases significantly as the angle of incidence becomes more horizontal, in particular for P and SV waves.

ACKNOWLEDGEMENTS

This work was supported by the Ministerio de Ciencia e Innovación of Spain (Subdirección General de Proyectos de Investigación) through research project BIA2010–21399–C02–01 and co–financed by the European Fund of Regional Development (FEDER). It was also supported by the Agencia Canaria de Investigación, Innovación y Sociedad de la Información (ACIISI) of the Government of the Canary Islands, through research project ProID20100224 (co-financed by FEDER) and through the research fellowship TESIS20100084, whose recipient is José M. Zarzalejos, and by FEDER funds. The authors would like to thank for this support.

References

[1] O'Rourke MJ, Bloom MC, Dobry R. Apparent propagation velocity of body waves. *Earthquake Eng Struct Dyn* 1982; **10**:283–294.

[2] Mamoon SM, Ahmad S. Seismic response of piles to obliquely incident SH, SV and P waves. *J Geotech Eng, ASCE* 1990; **116**:186–204.

[3] Mamoon SM, Banerjee PK. Response of piles and pile groups to travelling SH-waves. *Earthquake Eng Struct Dyn* 1990; **19**:597–610.

[4] Makris N, Badoni D. Seismic response of pile groups under oblique-shear and Rayleigh waves. *Earthquake Eng Struct Dyn* 1995; **24**(4):517–532.

[5] Kaynia AM, Novak M. Response of pile foundations to Rayleigh waves and obliquely incident body waves. *Earthquake Eng Struct Dyn* 1992; **21**:303–318.

[6] Gazetas G, Fan K, Tazoh T, Shimizu K, Kavvadas M, Makris N. Seismic pile-group-structure interaction. *Geotech Spec Publ, ASCE* 1992; **34**:56–93.

[7] Eurocode 8: Design of structures for earthquake resistance. Part 1: General rules, seismic actions and rules for buildings. Standard EN-1998-1, CEN/TC 250, 2003.

[8] Achenbach JD. *Wave propagation in elastic solids*. North-Holland:Amsterdam, 1973.

[9] Eringen AC, Suhubi ES. *Elastodynamics, volume 2 - Linear Theory*. Academic Press:NY, 1975.

[10] Veletsos AS, Meek JW. Dynamic behaviour of building-foundation systems. *Earthquake Eng Struct Dyn* 1974; **3**:121–138.

[11] Avilés J, Pérez-Rocha LE. Evaluation of interaction effects on the system period and the system damping due to foundation embedment and layer depth. *Soil Dyn Earthquake Eng* 1996; **15**:11–27.

[12] Avilés J, Pérez-Rocha LE. Effects of foundation embedment during building-soil interaction. *Earthquake Eng Struct Dyn* 1998; **27**:1523–1540.

[13] Padrón LA, Aznárez JJ, Maeso O. 3-D boundary element-finite element method for the dynamic analysis of piled buildings. *Eng Anal Bound Elem* 2011; **35**(3):465–477.

[14] Domínguez J. *Boundary elements in dynamics*. Computational Mechanics Publications & Elsevier Applied Science:Southampton, NY, 1993.

[15] Vanmarcke EH. *SIMQKE: A program for artificial motion generation*. Technical Report, Massachusetts Institute of Technology, Cambridge, MA, 1976.

[16] Kausel E, Ushijima R. Baseline correction of earthquake records in the frequency domain, Technical Report, Massachusetts Institute of Technology, 1979.

[17] Maeso O, Aznárez JJ, García F. Dynamic impedances of piles and groups of piles in saturated soils. *Comput Struct* 2005; **83**:769–782.

[18] Fan K, Gazetas G, Kaynia AM, Kausel E, Ahmad S. Kinematic seismic response of single piles and pile groups. *J Geotech Eng, ASCE* 1991; **117**:1860–1879.

[19] Montoya J, García Meseguer A, Murán Cabré F, Arroyo Portero J. *Hormigón armado, 15th edition*. Gustavo Gili:Barcelona, 2009.

[20] Eurocode 2: Design of concrete structures. Part 1: General rules, seismic actions and rules for buildings. Standard BS EN 1992-1-1, CEN/TC 250, 2004.

[21] Nikolaou S, Mylonakis G, Gazetas G, Tazoh T. Kinematic pile bending during earthquakes: analysis and field measurements. *Géotechnique* 2001; **51**:425–440.